Spectral response of the energy-binning Dosepix ASIC coupled to a 300 μm silicon sensor under high fluxes of synchrotron radiation

CrossMark

E. Fröjdh [a,b,*], F. Bisello [c,d], M. Campbell [a], J. Damet [a,e], E. Hamann [f], T. Koenig [f], W.S. Wong [a,e], M. Zuber [f]

[a] CERN, Geneva, Switzerland
[b] Mid Sweden University, Sundsvall, Sweden
[c] IBA Dosimetry GmbH, Schwarzenbruck, Germany
[d] FAU University Erlangen-Nrnberg, Erlangen, Germany
[e] Institute of Radiation Physics, Lausanne University Hospital, Lausanne, Switzerland
[f] ANKA Synchrotron Radiation Facility, KIT, Karlsruhe, Germany

ARTICLE INFO

ABSTRACT

The Dosepix hybrid pixel detector was designed for dosimetry and radiation monitoring applications. It has three programmable modes of operation: photon counting mode, energy integration mode, and dosimetry mode. The dosimetry mode measures the energy of individual X-ray photons and automatically sorts events into pre-defined energy bins. The output is a histogram representing the measured X-ray energy spectrum, permitting a dose reconstruction that accounts for the attenuation of photons at each energy bin. This presents a potential radiation protection and dosimetry instrument in medical radiodiagnostic practices, including high flux systems such as computed tomography (CT). In this paper, we characterise the Dosepix chip by investigating the energy response and count rate capabilities when coupled to a 300 μm silicon sensor under high fluxes of monochromatic synchrotron radiation. Under nominal settings, the Dosepix detector can detect photons down to 3.5 keV, with an energy resolution of 16.5% FWHM for 8.5 keV photons and 8% FWHM for 40 keV photons. The chip can count up to 1.67 Mcps/mm^2 of 40 keV photons whilst maintaining linear counting behaviour. This count rate range can be further increased by changing the programmable operating settings of the detector, making it suitable for a range of photon dosimetry applications.

1. Introduction

1.1. The dosepix detector

The Dosepix hybrid pixel detector consists of an application specific integrated circuit (ASIC) connected to a segmented semiconductor radiation sensor [1]. Both ASIC and sensor are segmented into 16 rows by 16 columns of square pixels with 220 μm pixel pitch. The ASIC and sensor were developed as two discrete modules that were separately optimized and combined as a hybrid detector assembly by bump-bonding. This hybridisation permits a choice in appropriate sensor material depending on application. For example, a high-Z (i.e. highly absorbing) sensor material such as CdTe ($Z_{Cd}=48$, $Z_{Te}=52$) would be well suited for the absorption of energies typically used in medical CT (the maximum tube

voltages, kVp, of medical CT scans typically generate X-ray spectra up to 120 keV–140 keV). Silicon ($Z_{Si}=14$) is a lower density material that efficiently absorbs photon energies up to roughly 20 keV; Si can still be used to detect photons of much higher energies but the absorption efficiency drops significantly. Nevertheless, due to the reliability and cost of silicon sensors, they are useful for detector characterization, which is the goal of this work. In this paper, we used a Dosepix detector assembly where the ASIC was connected to a 300 μm silicon sensor with 12 rows of full-sized 220×220 μm^2 pixels, and four special rows of reduced-area 55×55 μm^2 pixels.

Each Dosepix ASIC pixel contains an analogue frontend that outputs a voltage pulse whose height and width are proportional to the energy absorbed by the detector when an X-ray photon impinges on the corresponding sensor segment. This voltage pulse is compared to an analogue threshold voltage programmed to correspond to a given energy during calibration. Measuring the pulse width by counting the number of 100 MHz clock cycles

---

coincident with the time-over- threshold (TOT) signal gives a digital value that represents the photon energy absorbed in the sensor segment. In dosimetry mode, each pixel contains a 12-bit TOT counter and sixteen 16-bit counters that correspond to individually programmable digital thresholds. Since the chip contains 256 discrete channels, each with sixteen programmable thresholds, the detector can theoretically output photon spectra quantised in up to 3840 energy bins from 3.5 keV to roughly 1 MeV[1] (16 thresholds gives 15 bins + 1 overflow bin). Depending on the photon fluence, the combined area of several pixels is typically needed for each energy range in order to gather enough statistics to output sensible spectra. In this work, we divided the 16 columns into groups of four, and used four sets of digital thresholds to provide X-ray spectra measurements sampled into 60 unique energy bins. Because up to 65k hits per bin can be stored in the memory of each pixel, the spectrum of an X-ray beam can be measured in a single shot by the Dosepix detector (i.e. without the need for time-consuming threshold scans).

1.2. Pulse pileup and count rate linearity in photon counting systems

Single photon processing hybrid pixel detectors, such as the Dosepix detector, discretely process the signal from each detected photon. The advantages of single photon processing (compared to traditional energy integrating detectors) include the suppression of false signals due to electronics noise, and the ability to measure the energy of individual photons. The first point permits the detection of low energy X-rays down to a few keV. The second point is particularly important for X-ray dosimetry, as the absorption efficiency of photons in sensor materials (such as silicon) and in tissue, depends on the photon energy. Since X-ray tubes used in medicine output a broad energy spectra rather than monochromatic radiation, it is necessary to know the energy of the photons absorbed in a dosimeter in order to accurately calculate the equivalent dose in tissue. On the other hand, the time to process a pulse generated by an absorbed photon incurs a dead time, which is a drawback to evaluating each photon discretely. The Dosepix frontend can be described with the so-called paralysable detector model with respect to pulse pileup [2], which means that there can be an accumulation of multiple photons being processed concurrently by a single pixel. In such a system, individual photon events cannot be distinguished and this distorts the energy response of the detection system. The count rate linearity of a paralysable photon counting detector depends on many factors, including the pixel active area and the preamplifier reset current in the analogue frontend. Fig. 1 shows pileup scenario simulations of the output of the Dosepix preamplifier and analogue signal discriminator with various preamplifier reset currents. Preamplifier output pileup occurs when discrete input from the sensor arrives in intervals shorter than the processing time of a single input, which is inversely proportional to the preamplifier reset current. However, there is a practical trade-off between pileup reduction and energy resolution, as frontend noise increases with reset current and shorter pulses increase quantisation error in TOT photon energy measurements. The Dosepix frontend was designed for a nominal reset current of 2–3 nA, which can be programmed to a maximum value of 14.5 nA.
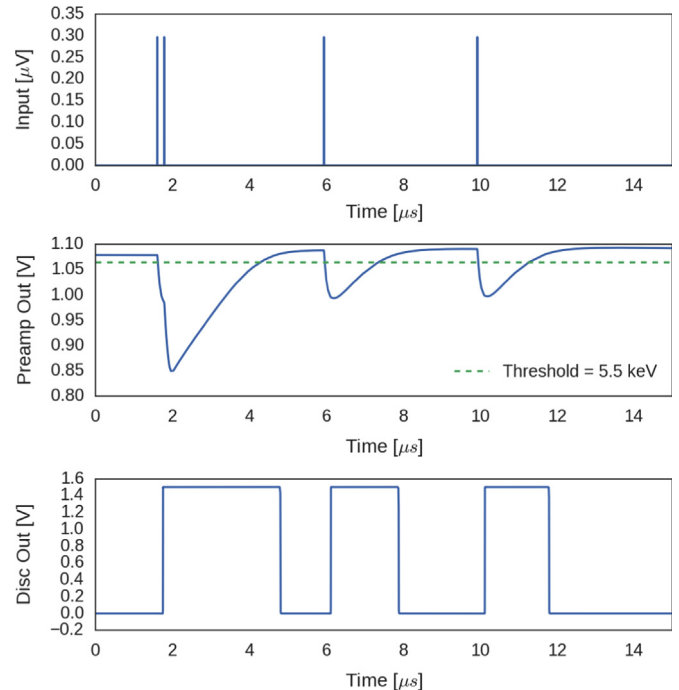
Fig. 1. Pileup scenario simulations of preamplifier and analogue discriminator output pulses from monochromatic 40 keV photons on a Si sensor. When pileup occurs, the outputs of several monochromatic photons are combined, distorting the detector energy response leading not only to higher energy counts but also lower energy counts if the next pulse sits on the undershoot of the previous pulse. *Note*: The preamplifier output pulse is inverted in this frontend.

1.3. Outline

This paper evaluates the performance of a Dosepix detector assembly equipped with a 300 μm silicon sensor. All experiments were carried out at the TopoTomo beamline of the ANKA Synchrotron Radiation Facility of the Karlsruhe Institute of Technology at varying photon fluxes. The monochromatic energy spectrum was provided by a double-multilayer monochromator ranging between 6 and 40 keV with an energy resolution of $\Delta E/E = 10^{-2}$.

Following this introduction, the paper is divided into five main content sections. Section 2 describes the simulation tools used to simulate energy response and pile up performance. Section 3 reports the energy resolution of a Dosepix detector. Section 4 discusses the calibration of the detector using electronics noise and monochromatic synchrotron radiation. Section 5 presents high flux measurements with synchrotron radiation. The paper will then conclude with a summary of the main values extracted from the chip characterisation and comments on future work.

2. Simulations

Two different simulation tools were used in this work. For the energy response of the detector presented in Fig. 4 the Geant4 extension geant4medipix [3] was used. This is a module that adds charge transport in the sensor layer using a pixel weighting field as well as a model for the pulse processing in the frontend. It also provides an easy to use framework to set up the experiment geometry and to vary the pixel and detector dimensions. Looking at the results presented in Fig. 4 we observe more charge sharing in the measurements than in the simulation. This discrepancy is believed to come mostly from an underestimation of the charge sharing in the simulations, which is consistent with results when simulating other detectors in the Medipix family using the same

software. A minor contribution could come from scattering from the other detectors in the set-up since the measurements were done using wide beam.

Although geant4medipix has an implementation of the pulse processing it is a simplified model built on a convolution with a preamplifier response function, and does not currently handle multiple events at the same time. To simulate pulse pileup in the front end the Analogue Design Environment from Virtuoso was used with a model of Dosepix. This model gives a more complete representation of the frontend. As input to the simulation square pulses of 5 ns, arriving randomly with the specified rate were used. The results of the pileup simulations is included in the two Figs. 6 and 7 and in Table 4.

3. Energy resolution of a dosepix detector with a 300 μm si sensor

Electrical measurements of a bare Dosepix ASIC (i.e. without sensor) were previously reported by Wong et al. [4]. Characterization using X-ray tubes, XRF and radioactive sources can be found in the articles published by Ritter et al. [5] and Zang et al. [6]. In this paper we discuss the energy resolution of a Dosepix detector assembly consisting of the ASIC bump-bonded to a 300 μm Si sensor subject to monochromatic synchrotron radiation. A set of digital-to-analogue-converters (DACs) in the chip periphery programs the operational bias points of the pixel analogue frontend circuits. The IKRUM[2] DAC selects the reset current of the frontend preamplifier, which determines the time to return the preamplifier output voltage to baseline, and also affects the frontend gain (which in turn affects the equivalent noise charge) [1]. In this work, we compare the Dosepix assembly performance with IKRUM DAC settings of 15 and 60, which correspond to preamplifier reset currents of 2.6 nA and 7.4 nA, respectively. The remainder of the chip operation DACs were programmed to supply each pixel frontend with 13.5 μW. Table 1 lists the equivalent noise charge (ENC) of the frontend electronics based on these DAC settings and based on the pixel area (the ENC depends in the frontend input capacitance, which is a function of the sensor area).

Table 2 reports the energy resolution in terms of the full-width at half maximum (FWHM) in TOT mode with a 100 MHz clock, of monochromatic synchrotron radiation ranging from 8.5 keV to 40 keV, which was the range of energies available at the beamline. There is a slight degradation in the energy resolution in the reduced-area pixels due to charge sharing in the segmented sensor.

4. Energy calibration of the dosepix detector

The absorbed energy corresponding to the measured number of TOT counts varies between pixels due to analogue threshold and frontend gain mismatch [1]. Because the Dosepix detector sorts events into energy bins directly during measurement, it is necessary to pre-define the energy bins by determining the appropriate set of programmable digital thresholds through energy calibration of the Dosepix detector.

In order to set a low global analogue threshold (which also sets the lower limit of the digital thresholds), we first performed an analogue threshold equalisation procedure to minimise threshold dispersion. We then followed the TOT calibration method developed for the Timepix ASIC of the Medipix2 Collaboration [8] to

---

Table 1
Electronics noise of the Dosepix frontend (with 300 μm Si sensor) measured for the two different pixel sizes.

IKRUM	σ_{ENC}, rms (e$^-$)	
[Code] [nA]	$220 \times 220 \, \mu m^2$	$55 \times 55 \, \mu m^2$
15 (2.6)	161	134
60 (7.4)	193	162

determine a TOT versus energy relationship for each pixel. Finally, we used the dpxctrl software to calculate the set of digital thresholds (in units of 100 MHz TOT counts) for each pixel based on the TOT-to-energy relationship.

4.1. Analogue threshold equalisation

The total set of pixels has an inherent dispersion of the global analogue threshold voltage due to transistor mismatch and voltage drop along pixel columns. This dispersion limits the minimum level at which the analogue threshold can be set, thereby limiting the detection of soft X-rays. It also pushes the non-linear region of the TOT-to-energy relationship (see Section 4.2) towards higher energy ranges. The minimum analogue threshold is given by

$$TH_{min}[keV] \approx 6\epsilon_i \sqrt{(\sigma_{ENC}^2 + \sigma_{th}^2)} \qquad (1)$$

where the average ionisation energy, ϵ_i, in silicon is approximately 3.62 eV at 300 K [2]. To reduce the threshold dispersion, each Dosepix frontend contains a programmable, in-pixel threshold trimming DAC to locally tune the analogue threshold voltage. Analogue threshold equalisation is the method to determine the appropriate trim code for each pixel based on the local threshold offset. It can be done using electronics noise, using programmable charge injection into the frontend (i.e. analogue test-pulses), or using a source of monochromatic ionising radiation. Table 3 presents the analogue threshold dispersion before and after threshold tuning using electronics noise to calculate the appropriate trim code for each pixel.

4.2. TOT-to-energy calibration

Fig. 2 shows the energy response of a single pixel with a 100 MHz TOT clock and analogue threshold of 5.5 keV for two different IKRUM vales, measuring monochromatic synchrotron radiation at the energies listed in Table 2. Note that the preamplifier output pulses are much shorter with the higher reset current.

The spread in the 256 curves corresponding to the calibration curves of all the single pixels of the detector in Fig. 3 is due to residual threshold offset and frontend gain variation (due to transistor mismatch, voltage drop along pixel columns, and different input capacitances from the different pixel sizes). This spread between pixels can then be corrected during regular operation of the detector by programming unique digital thresholds into each pixel, calculated based on their respective TOT calibration curves.

The empirical surrogate function describing a TOT-to-energy calibration curve is given by [8]:

$$f(x) = ax + b - \frac{c}{x-t} \qquad (2)$$

where x is the photon energy (i.e. horizontal axis), a is the slope of the linear region, b is the y intercept of the linear region, and $c/(x-t)$ describes the region below the knee. The dpxctrl software extrapolates the calibration curve for each pixel and calculates the appropriate TOT values of digital thresholds.
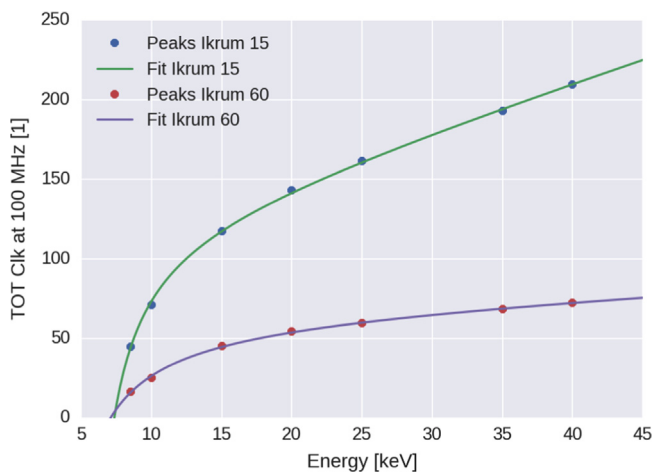
Table 2
Energy resolution of Dosepix assembly in TOT mode using a 100 MHz clock (with 300 μm Si sensor).

| Energy | Energy resolution, FWHM Regular-sized, 220 × 220 μm^2 pixels | | | | Reduced-area, 55 × 55 μm^2 pixels | | | |
| | IKRUM=15 | | IKRUM=60 | | IKRUM=15 | | IKRUM=60 | |
(keV)	(keV)	%	(keV)	%	(keV)	%	(keV)	%
8.5	1.43	16.8	2.17	25.5	1.70	20.0	2.29	26.9
10	1.66	16.6	2.17	21.7	1.88	18.8	1.69	16.9
15	2.40	16.0	2.35	15.7	2.28	15.2	2.11	14.1
20	2.81	14.0	2.91	14.6	2.86	14.3	3.22	16.1
25	2.90	11.6	3.17	12.7	2.96	11.8	3.39	13.5
35	3.12	8.92	3.62	10.3	3.18	9.08	4.04	11.5
40	3.18	7.95	3.79	9.48	3.56	8.90	4.53	11.3

Table 3
Analogue threshold dispersion of a Dosepix assembly (with 300 μm Si sensor).

IKRUM	Trim code 0 × 0 in all pixels	Optimized trim code per pixel
σ_{th}, rms [e$^-$]		
15	1013	26.6
60	1252	37.2
Threshold$_{min}$ [keV]		
15	22.3	3.54
60	27.2	4.27

Fig. 2. TOT calibration curve for one pixel (8, 8) with IKRUM=15 (2.6 nA) and IKRUM=60 (7.4 nA).
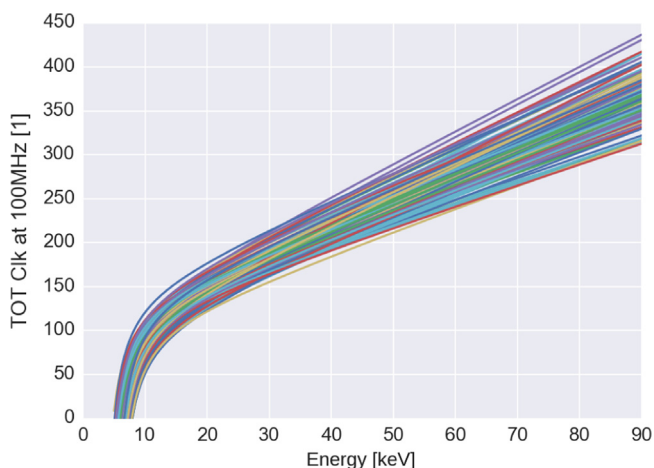
Fig. 3. TOT calibration curves of all pixels in the matrix extrapolated to 90 keV to highlight the gain spread (IKRUM=15).
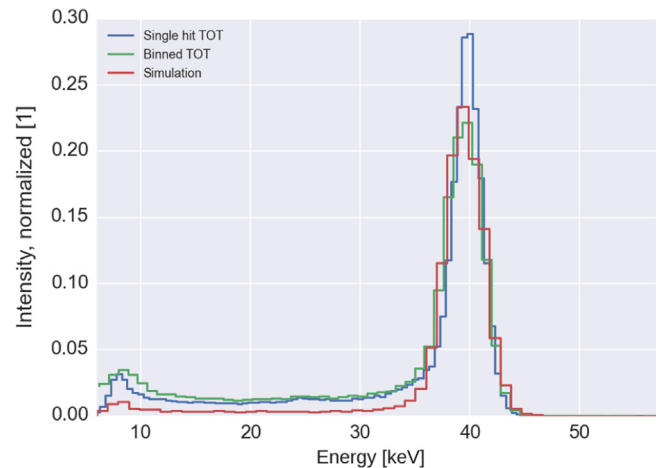
Fig. 4. Measured spectrum in energy binned mode and single hit TOT mode using IKRUM 15, compared with a simulation performed in geant4medipix [3].

For the measurements in this work, we programmed the Dosepix detector with 60 equidistant energy bins from 5.5 keV to 64 keV, and an extended range of 5.5 keV to 150 keV to study pileup effects.

4.3. Binned energy measurements from a calibrated detector

To demonstrate the results of the detector calibration, Fig. 4 shows the raw output of the Dosepix detector in a beam of monochromatic 40 keV photons. In this measurement, the digital thresholds were programmed to define 60 unique energy bins from 5.5 keV to 64 keV. The binned peak has a resolution of 4.3 keV FWHM. The slight degradation in energy resolution in binning mode (compared to the resolution reported for raw TOT counts in Section 3) is due to event quantisation in the discrete bins. The counts below 40 keV are due to charge sharing in the pixels, and the bump at 8 keV is from X-ray fluorescence of copper from the bump bonds.

5. High flux measurements with monochromatic synchrotron radiation

5.1. Count rate linearity

The count rate linearity for the Medipix3RX detector of the Medipix3 Collaboration was previously reported by Fröjdh et al. for silicon [9] and by Koenig et al. for CdTe [10]. Recently Zang et al. [6] presented a count rate study of Dosepix for both detector materials using a polychromatic spectrum . In this work, we followed similar steps as for the Medipix3RX characterization to

determine the count rate linearity of a Dosepix detector coupled to a 300 μm Si sensor, counting the number of photons from monochromatic synchrotron radiation beams of 17 keV, 30 keV, and 40 keV. These energy points were selected as energies of interest for quality assurance routines of mammography imaging systems, and mean energies for the reference X-ray beam qualities recommended by the International Electrotechnical Commission (IEC) for medical imaging: RQR5 and RQR7 [11]. 40 keV was also the highest beam energy available in our experimental setup. The input photon flux was adjusted using Al filters and by using different parts of the non-homogeneous beam. The analogue threshold was set to 5.5 keV and the chip operated in energy binning mode with the lowest bin set at 0 TOT in all pixels. The counts in this bin was then used for the count rate fit. Fig. 5 shows the photon counting intensity profile of the beam at 40 keV and low flux. Due to the limited statistics recorded in the four rows of 55 μm pitch pixels, the characterisation of the count rate linearity will be based on results from the 12 rows of pixels with the 220 μm native pitch. From measurements with Medipix3RX [9] we also do not expect a significant difference between the different pixel sizes, except a factor 16 coming from the pixel area.

Figs. 6 and 7 shows the measured count rates with the Dosepix detector placed in a beam of monochromatic 40 keV photons for two values of IKRUM. The input count rate was calculated from the region with linear response and represent the pulses that the chip sees. The output count rate (i.e. the counts recorded by the Dosepix electronics) follows the input count rate at low input fluxes. For high input fluxes, the output count rate deviates from the input count rate due to pulse pileup in the frontend. The frontend simulations generally agrees well with the measurements for the low IKRUM settings but shows longer dead-times for the higher IKRUM settings. Still we see it as a valuable tool for predicting pileup response in hybrid pixel detectors. Ideally the detailed frontend simulation should be connected to a sensor simulation (such as geant4medipix) to be provided with more realistic input pulses.

These measurements were repeated for 30 keV and 17 keV photons. To determine the photon processing dead-time, we used a simple paralysable detector model to fit the recorded count rate m, as a function of input count rate n, and extract the dead-time, τ [2]:
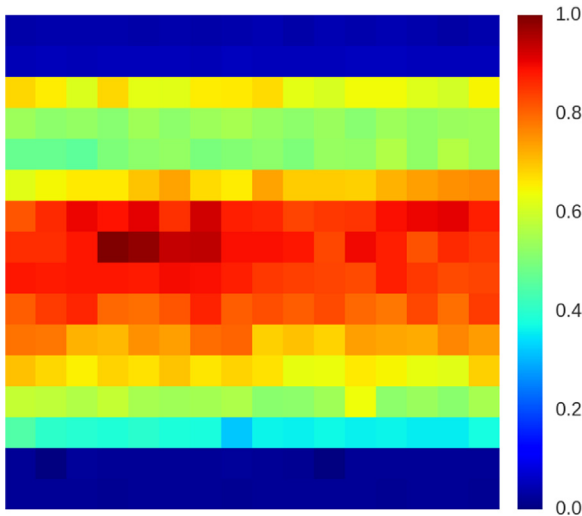
$$m = ne^{-\tau n} \tag{3}$$

Fig. 5. Relative intensity of the beam as measured by Dosepix at 40 keV. Note that the low intensity in the top two and bottom two rows is due to the smaller (55 × 55 μm²) pixels while the variations in the centre originates from the beam.

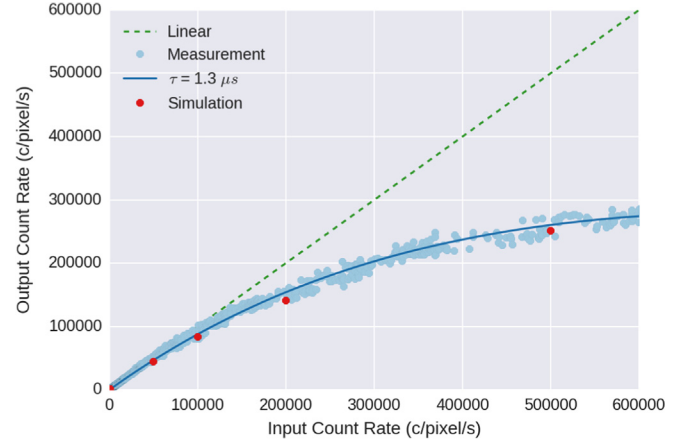**Fig. 6.** Recorded counts of 40 keV synchrotron radiation, using the 220 × 220 μm² pixels with IKRUM = 15. The figures also includes the fitted dead time according to Eq. (3) and simulated count rates using the method described in section.
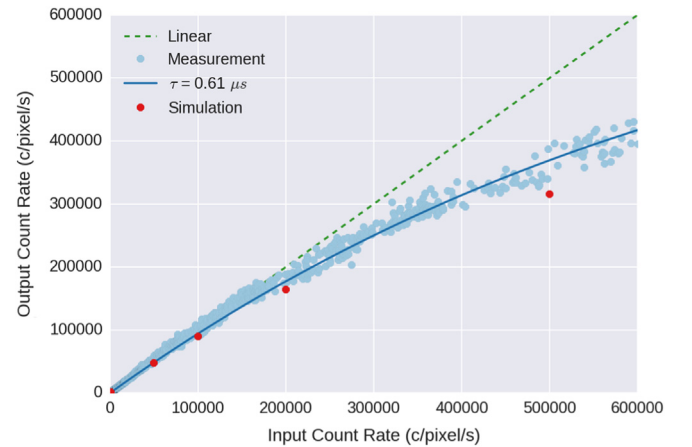

Fig. 7. Recorded counts of 40 keV synchrotron radiation, using the 220 × 220 μm² pixels with IKRUM = 60. Analogue threshold = 5.5 keV. The figures also includes the fitted dead time according to Eq. (3) and simulated count rates using the method described in section.

We calculate the 10% deviation point ($I_{0.9}$) from linear response using the fitted dead-time (τ). This gives a figure of merit for the rate that the chip can handle. At this point we observe a spectral distortion and pileup counts but the overall shape of the spectrum is intact. It is important to note that the maximum linear count rate is based on the flux at the input of the electronics, which is the flux absorbed by the sensor material. The actual incident flux from the beam, I_{photon}, depends on the attenuation at the photon energy [2]:

$$I = I_{photon}e^{-\mu t} \tag{4}$$

where, in the case of this work, μ is the linear attenuation coefficient of photons in silicon at a given energy, and t is the sensor thickness (300 μm). Table 4 lists the dead-time, 10% deviation point, and incident beam flux at the 10% deviation point for our set of measurements. Simulations of the frontend are also presented and include the case where IKRUM is the maximum programmable DAC code of 255 (14.5 nA).

5.2. Spectral response at high flux

Fig. 8 shows that, at low fluxes, the Dosepix detector correctly measures the photopeak at 40 keV in energy binned mode. However at high fluxes, the photopeak moves towards lower energies

and false high energy counts are recorded above the incident photon energy due to pulse pileup in the analogue frontend. Although we can model and correct for the deviation in count rates in photon counting applications, we unfortunately cannot recover from pileup distortions in the spectral response [9].

Table 4
Measurement and frontend simulation of processing dead-times (τ) and count rate at 10% deviation from linear. $I_{photons}$ is the actual number of incoming photons as the 10% point calculated using Eq. (4).

Energy (keV)	IKRUM (Code)	Measurement with detector			Frontend simulation	
		τ (μs)	$I_{0.9}$ (Mcp/mm^2)	I_{photon} (Mcp/mm^2)	τ (μs)	$I_{0.9}$ (Mcp/mm^2)
17	15	1.23	1.77	4.99	1.34	1.62
	60	0.50	4.35	12.3	0.82	2.65
	255	–	–	–	0.64	3.40
30	15	1.29	1.69	19.7	1.27	1.71
	60	0.53	4.11	47.8	0.89	2.45
	255	–	–	–	0.71	3.07
40	15	1.3	1.67	38.8	1.40	1.55
	60	0.61	3.57	83.0	0.93	2.34
	255	–	–	–	0.73	2.98

6. Conclusions and future work

We have characterised the energy response and high flux count rate capabilities of a Dosepix detector coupled to a 300 μm Si sensor . Because photon attenuation in semiconductor sensors as well as biological tissue depend on photon energy, the spectral information provided by Dosepix permits a means to reconstruct dose that accounts for photon attenuation in each energy bin. However, the processing dead-time required to compute the energy of each absorbed photon on-chip limits the input fluxes that the ASIC can handle. These limits have been characterised in this work in order to provide a guideline on the appropriate use of the Dosepix detector. Under nominal chip settings, the Dosepix energy resolution in energy binning mode was measured to be 16.5% FWHM for 8.5 keV photons and 8% FWHM for 40 keV photons, and the maximum linear count rate was measured to be 1.67 Mcps/mm^2 for 40 keV photons.

The results presented in this chip characterisation paper indicate that Dosepix could be a promising device for dosimetry applications in the medical field, particularly since dosimeters are not typically placed directly in beams and are therefore required to detect lower fluxes than imaging detectors. The next step, therefore, is to use Dosepix in operational radio protection and dosimetry applications that can benefit from a detector that measures X-ray energy spectra in a single acquisition, for example, the
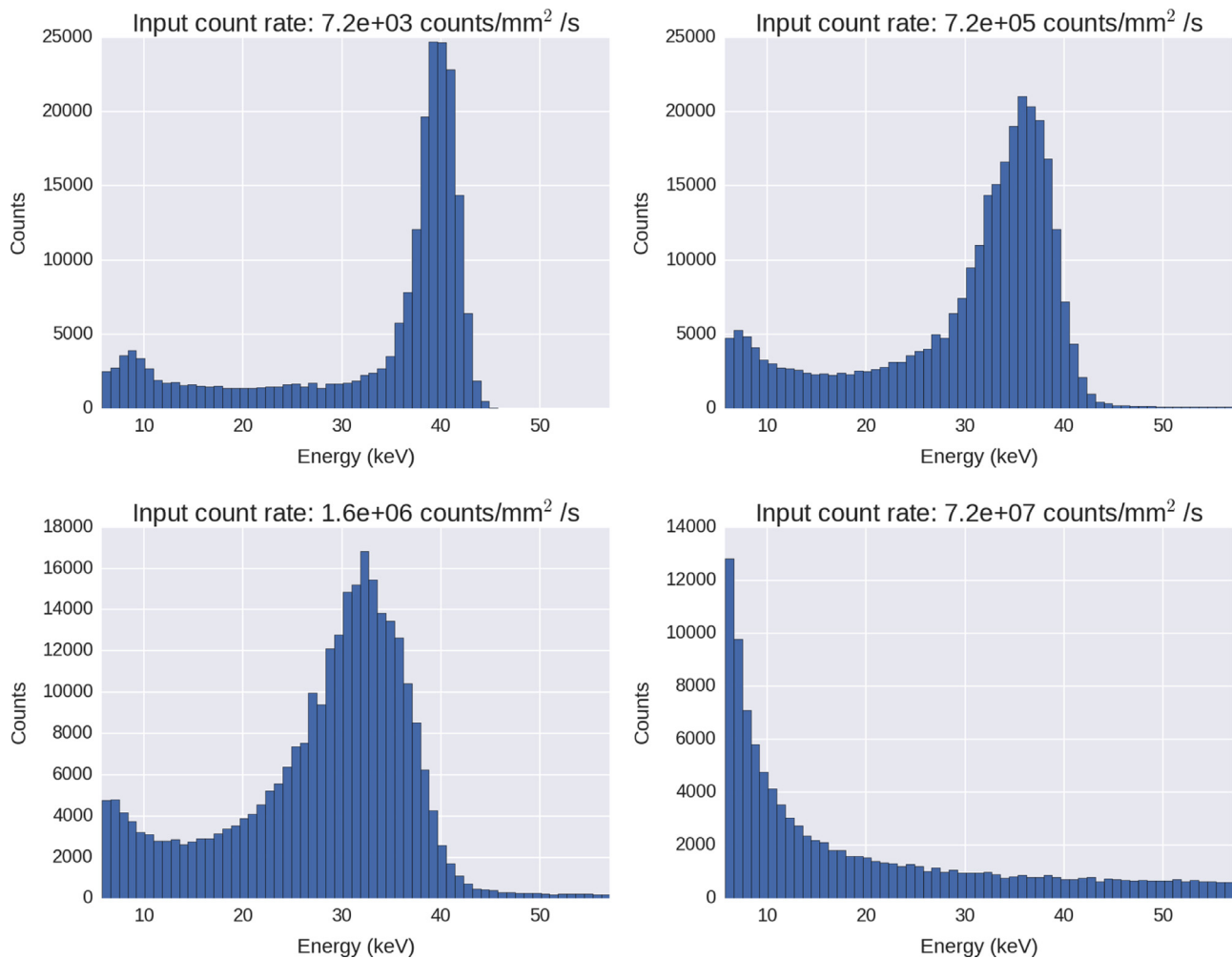
Fig. 8. Energy response measuring 40 keV photons at various measured input fluxes in the 220 × 220 μm^2 pixels of the Dosepix detector using IKRUM=15. *Note:* These are not results of threshold scans. The data shown here was measured in a single acquisition in energy binning mode using calibrated energy bins programmed from 5.5 keV to 64 keV in 60 bins.

characterization of background scatter radiation in a radiological room and dosimetric workplace study for the medical staff.

Acknowledgements

References

[1] W. Wong, A hybrid pixel detector ASIC with energy binning for real-time, spectroscopic dose measurements (Ph.D. thesis). Mid Sweden University, 2012.

[2] G.F. Knoll, Radiation Detection and Measurement, 4th Edition, John Wiley & Sons, 2010.

[3] A. Schübel, D. Krapohl, E. Fröjdh, C. Fröjdh, G. Thungström, Journal of Instrumentation 9 (12) (2014) C12018, http://dx.doi.org/10.1088/1748-0221/9/12/C12018.

[4] W.S. Wong, G. Anton, R. Ballabriga, G. Blaj, M. Böhnel, M. Campbell, T. Gabor, E. Heijne, X. Llopart, T. Michel, I. Ritter, T. Poikela, P. Sievers, L. Tlustos, P. Valerio, Journal of Instrumentation 7 (01) (2012) C01056, http://dx.doi.org/10.1088/1748-0221/7/01/C01056.

[5] I. Ritter, G. Anton, R.B. Sune, F. Bisello, M. Campbell, T. Gabor, X.L. Cudie, S. Wölfel, W.S. Wong, T. Michel, Journal of Instrumentation 9 (05) (2014) C05069, http://dx.doi.org/10.1088/1748-0221/9/05/C05069.

[6] A. Zang, G. Anton, R. Ballabriga, F. Bisello, M. Campbell, J. Celi, A. Fauler, M. Fiederle, M. Jensch, N. Kochanski, X. Llopart, N. Michel, U. Mollenhauer, I. Ritter, F. Tennert, S. Wölfel, W. Wong, T. Michel, Journal of Instrumentation 10 (04) (2015) C04015, http://dx.doi.org/10.1088/1748-0221/10/04/C04015.

[7] F. Krummenacher, Nuclear Instruments and Methods in Physics Research Section A: Accelerators, Spectrometers, Detectors and Associated Equipment 305 (3) (1991) 527, http://dx.doi.org/10.1016/0168-9002(91)90152-G.

[8] J. Jakubek, Nuclear Instruments and Methods in Physics Research Section A: Accelerators, Spectrometers, Detectors and Associated Equipment 633 (2011) S262, http://dx.doi.org/10.1016/j.nima.2010.06.183.

[9] E. Frojdh, R. Ballabriga, M. Campbell, M. Fiederle, E. Hamann, T. Koenig, X. Llopart, D.d.P. Magalhaes, M. Zuber, Journal of Instrumentation 9 (04) (2014) C04028, http://dx.doi.org/10.1088/1748-0221/9/04/C04028.

[10] T. Koenig, E. Hamann, S. Procz, R. Ballabriga, A. Cecilia, M. Zuber, X. Llopart, M. Campbell, A. Fauler, T. Baumbach, M. Fiederle, IEEE Transactions on Nuclear Science NS-60 (6) (2013) 4713, http://dx.doi.org/10.1109/TNS.2013.2286672.

[11] IEC, Medical diagnostic X-ray equipmentRadiation conditions for use in the determination of characteristics, IEC 61267 ed 2.0, 2005.